ChemPubSoc Europe

DOI: 10.1002/chem.201901494

CHEMISTRY A European Journal Full Paper

Supramolecular Chemistry |*Hot Paper*|

Sequence and Structure of Peptoid Oligomers Can Tune the Photoluminescence of an Embedded Ruthenium Dye

Lieby Zborovsky, Hagar Tigger-Zaborov, and Galia Maayan*[a]

Abstract: The understanding of structure–function relationships within synthetic biomimetic systems is a fundamental challenge in chemistry. Herein we report the direct correlation between the structure of short peptoid ligands—N-substituted glycine oligomers incorporating 2,2′-bipyridine groups—varied in their monomer sequence, and the photoluminescence of Ru^{II} centers coordinated by these ligands. Based on circular dichroism and fluorescence spectroscopy we demonstrate that while helical peptoids do not affect the fluorescence of the embedded Ru^{II} chromophore, unstructured peptoids lead to its significant decay. Transmittance electron microscopy (TEM) revealed significant differences in the arrangements of metal-bound helical versus unstructured peptoids, suggesting that only the latter can have through-space interactions with the ruthenium dye leading to its quenching. High-resolution TEM enabled the remarkable direct imaging of singular ruthenium-bound peptoids and bundles, supporting our explanation for structure-depended quenching. Moreover, this correlation allowed us to fine-tune the luminescence properties of the complexes simply by modifying the sequence of their peptoid ligands. Finally, we also describe the chiral properties of these Ru–peptoids and demonstrate that remote chiral induction from the peptoids backbone to the ruthenium center is only possible when the peptoids are both chiral and helical.

Introduction

The relationship between structure and function is well established in biological systems, leading to the unique properties of natural polymers. Mimicking such structure–function relationships requires the design of versatile sequences that: i) include functional groups such as metal-binding ligands,[1] catalysts and chromophores, and ii) enable control over secondary structures, such as helices. Helical metal-binding scaffolds can further form enantiopure metal complexes, with a wide potential in cooperative and asymmetric catalysis,[2] material science and chemical biology.[3]

Peptoids, oligomers of N-substituted glycine, are peptidomimetics that can adopt helical secondary structures with a helical pitch of three residues per turn if bulky chiral side chains are incorporated within their sequence.[4] The helicity of peptoids can be easily modified by utilizing different side-groups, forming secondary structures with different degrees of helicity, thus making them excellent candidates for studying the interplay between structure and function.[5] It was previously reported, for example, that single-handed peptoid helices could induce chirality at an embedded achiral catalyst for applications in asymmetric catalysis.[6] Thorough sequence–structure–function studies revealed that the enantioselectivity of the catalytic peptoids strongly depends on the degree of conformational order of the scaffold.[6] It was also demonstrated that the luminescence intensity of synthetic helicates,[7,8] aromatic foldamers,[9] peptides[10] and peptoids[11] containing chromophores incorporated in their backbone, could be controlled by changing the chemical environment of the chromophore using solvophobic interactions,[9] pH,[11b] or binding of substrate molecules.[12] However, the direct relationship between the conformational order of peptidomimetics and a physical utility such as the luminescence of an embedded metal complex, that does not involve changing its chemical environment, has not yet been reported. Linking together two fundamental properties such as high-order structure and luminescence may provide fundamental insights on the relationship between structure and function, and open new avenues for possible applications in photocatalysis, chemical biology, molecular imaging and more.

In an ongoing effort to understand the relationship between structure and function in synthetic systems, we have designed and synthesized a set of 13 short peptoid oligomers bearing 2,2′-bipyridine (bipy) ligand at their N terminus. In the other positions we placed only 1–6 chiral or achiral substituents, which are either known helix inducers or which cannot induce helix formation. We chose to incorporate $Ru(bipy)_3$ complexes within the peptoids due to their unique combination of chemical stability, excited state lifetimes and reactivity, and luminescence emission.[13] Thus, each peptoid was combined with Ru^{II}, and its structural, luminescence and chiral properties before and after Ru^{II} binding were investigated using circular dichroism (CD) and fluorescence spectroscopies as well as advanced

[a] *Dr. L. Zborovsky, Dr. H. Tigger-Zaborov, Prof. Dr. G. Maayan*
Technion-Israel Institute of Technology Haifa (Israel)
E-mail: gm92@tx.technion.ac.il

Supporting information and the ORCID identification number(s) for the author(s) of this article can be found under: https://doi.org/10.1002/chem.201901494.

high resolution electron microscopy (HR-TEM) techniques. Our studies revealed a unique correlation between the secondary structure of the peptoid ligand(s) and both the luminescence intensity and the chirality of the embedded ruthenium centers, which could be tuned simply by modifying the sequence of the peptoid ligands.

Results and Discussion

Design and synthesis of peptoid oligomers and their Ru^{II} complexes

The set of peptoids depicted in Figure 1 was synthesized on solid support from (*S*)- or (*R*)-1-phenylethylamine (*N*spe or *N*rpe, respectively), (*S*)-1-cyclohexylethylamine (*N*sch),[4d] (*R*)-1-*tert*-butylethylamine (*N*r1tbe),[4l] benzylamine (*N*pm), (*S*)-1-methoxypropylamine (*N*smp) and [(4"-methyl-2′,2"-bipyridine4′-yl)-methyl]oxy]ethylamine (*N*bpm) submonomer synthons in an efficient iterated two-step protocol.[14] It was previously shown that oligomers containing at least 66% of chiral bulky side chains, specifically *N*spe, *N*rpe, *N*sch or *N*s1tbe, out of all the substituents within the sequence, could fold into helical peptoid structures.[4] It was also demonstrated that the degree of helical character is elevated with increasing number of monomeric units.[4b] In contrast, peptoids incorporating a majority of *N*smp groups are unstructured,[15] and the introduction of achiral benzyl substituents within homo-oligomers of *N*spe decreases the degree of the peptoids helicity.[16] Thus, the set of peptoids in Figure 1 includes helical peptoids, chiral nonhelical peptoid, an achiral peptoid, *N*spe peptoids in different lengths, and *N*spe pentamers incorporating *N*pm groups varied in their number and position, which are anticipated to be varied in their degree of helicity.

It is known that substitution on the bipyridine ring strongly affects the photoluminescence properties of the obtained ruthenium complex.[17] Thus, *N*bpm was chosen because the peptoid binding linker is attached to the 6′-position and because the quantum luminescence efficiency of tri(4,4′-dimethyl-2,2′-bipyridyl) ruthenium complex is much higher than that of analogous complexes with (6,6′-dimethyl-2,2′-bipyridyl) or (5,5′-dimethyl-2,2′-bipyridyl) as ligands.[17] *N*bpm was synthesized by a two-step procedure starting from the commercially available 4,4′-dimethyl-2,2′-bipyridine as a precursor (see the Supporting Information). The *N*bpm group was placed at the N terminus of each peptoid aiming to explore the effect of different sequences and structures on the luminescence proper-

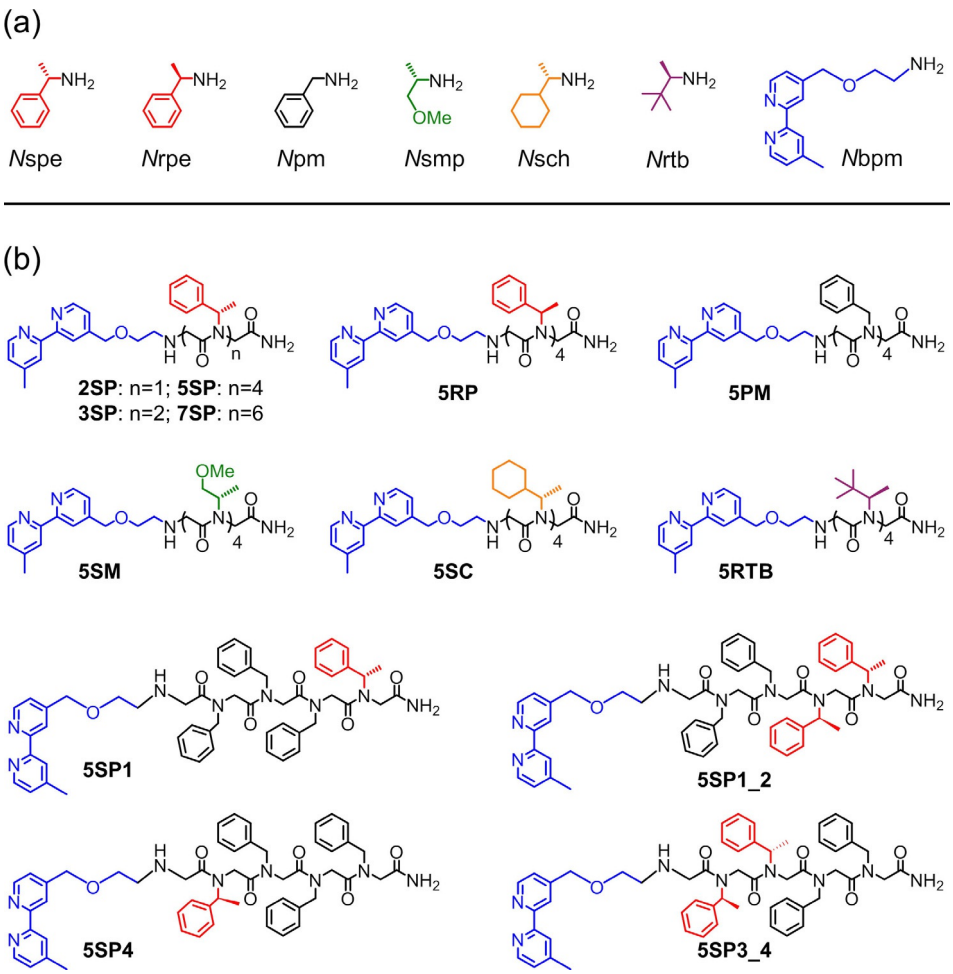

Figure 1. Peptoid oligomers for constructing Ru complexes. a) Monomeric units used in the design of the peptoids. b) Chemical sequences of peptoids studied in this work. Modular peptoid synthesis permits systematic control of the chain length, monomer type, and the position and number of chiral (colored, color choice arbitrary) and achiral (black) substituents.

ties of an embedded $Ru(bipy)_3(PF_6)_2$ complex. The modularity of the "sub-monomer" protocol permits the attachment of different substituents at defined positions along the peptoid backbone, enabling systematic structure–function investigations.[4] All peptoids were synthesized by the "sub-monomer" approach,[18] analyzed and purified by high-pressure liquid chromatography (HPLC, >95%). The molecular weights measured by electrospray ionization mass spectrometry (ESI-MS) were consistent with the expected masses (see the Supporting Information). The homoleptic Ru^{2+} complexes were prepared using a previously described procedure.[19] The complexes were precipitated with NH_4PF_6, centrifuged and separated. The Ru^{II}–peptoids complexes were analyzed and purified using HPLC (>95%) and their identity was verified by ESI-MS.

UV/Vis and emission spectroscopy

The metal-free peptoids exhibited absorption bands near $\lambda =$ 280 nm, in acetonitrile, corresponding to the π–π^* transition of the bipyridyl group (see the Supporting Information). The corresponding homoleptic Ru^{2+} complexes reveal a 5–10 nm shifts in this absorption band with a significantly increased intensity. In all cases, with the exception of Ru(**2SP**)$_3$ and Ru(**5SM**)$_3$, an additional band near $\lambda = 450$ nm, which corresponds to the metal-to-ligand charge transfer (MLCT) band of the ruthenium tribipyridine complex is observed[17] (Table 1). This band appears near $\lambda = 454$ and 445 nm for Ru(**2SP**)$_3$ and Ru(**5SM**)$_3$, respectively. Upon irradiation at 450 nm, in air, in acetonitrile, all the complexes show an emission band in the wavelength range of 545–800 nm indicating they are photoluminescent in solution. The luminescence energy of the Ru–peptoid complexes is red shifted by 13–19 nm compared with that of $Ru(bipy)_3(PF_6)_2$, which is 606 nm (Table 1, entry 1), and this is consistent with the red shift observed for the MLCT absorption band of the peptoid complexes.

Table 1. Experimental values of absorbance and emission maximal wavelength (λ_{max}), quantum luminescence efficiencies (Φ) and excited state lifetimes (τ) of peptoid complexes at RT, in acetonitrile, in air.

Entry	$Ru(L)_3$; L =	Absorbance (MLCT) λ_{max}	Emission λ_{max}	Φ[a]	τ (μs)
1	bipy	451	606	0.018[b]	0.156
2	**2SP**	454	625	0.005	0.141
3	**3SP**	459	619	0.015	0.164
4	**5SP**	460	620	0.017	0.187
5	**5RP**	461	625	0.016	0.187
6	**7SP**	460	622	0.019	0.189
7	**5SM**	445	625	0.002	0.128
8	**5PM**	462	625	0.006	0.150
9	**5SC**	460	621	0.022	0.187
10	**5RTB**	458	620	0.017	0.165
11	**5SP1**	459	623	0.017	0.171
12	**5SP1_2**	459	624	0.016	0.159
13	**5SP4**	460	623	0.011	0.167
14	**5SP3_4**	461	622	0.016	0.165

[a] Measured in ACN at RT in air. [b] Reference [20].

Circular dichroism (CD) spectroscopy of the peptoid pentamers

In contrast to polyproline peptides that are composed of either *cis* or *trans* amide bonds, peptoid monomers can favor both *cis* and *trans* orientation of the amide bond. This can be easily evidenced from CD spectroscopy, which is a key tool for describing the secondary structure of peptoids. It has been previously demonstrated that *N*spe, *N*rpe, *N*sch and *N*s1tbe substituted peptoids adopt right-handed helical structures akin to polyproline type-I (PP-I) helices.[4] The CD spectra of peptoids having only phenylethyl side chains (phenylethyl peptoids) exhibit a characteristic double minima (*N*spe) or a double maxima (*N*rpe) with bands near 200 nm and 220 nm, that are associated with *trans*-amide bond and *cis*-amide bond conformations, respectively.[4c] Peptoids containing only tertiary butyl groups or cyclohexyl groups, on the other hand, were shown to adopt all-*cis* PP-I helices and their CD spectra resemble these of PP-I peptide helices, with two minima near 190 and 225 nm and a maximum near 210 nm.[4l] The CD spectra of **5SP** and **5RP** having *N*spe or *N*rpe monomers, respectively, show the expected characteristic double minima or maxima with bands at 203 and 220 nm. The CD spectrum of **5SC** shows characteristic two minima at 196 and 222 nm and a maximum at 208 nm, and the spectra of **5RTB** exhibits two maxima at 198 and 223 nm and one minimum at 211 nm as was expected for oligomers that contain *N*sch and *N*r1tbe groups, correspondingly.[4l] The CD spectrum of **5SM** exhibits a minimum near 190 nm, characteristic of a chiral yet unstructured peptoid and **5PM**, being achiral, does not exhibit a CD spectrum (see the Supporting Information). In all cases, the CD spectra of Ru(pentamer)$_3$ complexes show bands in the 190–230 nm region that are similar to their corresponding unbound peptoid pentamers (Figure 2a).

Luminescence of the Ru–peptoid complexes

Although all the Ru(pentamer)$_3$ complexes show fluorescence emission (Table 1), we noticed an interesting and unique trend within the intensity of the emission; while the emission spectra of the ruthenium complexes of helical peptoids **5SP**, **5RP**, **5SC** and **5RTB** exhibit intensity very similar to this of $Ru(bipy)_3(PF_6)_2$ complex, the intensities of the emission spectra of the chiral unstructured Ru(**5SM**)$_3$ and the achiral Ru(**5PM**)$_3$ complexes are significantly lower (Figure 2b). We have also calculated the experimentally derived value of the luminescence quantum efficiency (Φ) of the Ru(pentamer)$_3$ complexes, based on their absorbance data at 450 nm and the integrated fluorescence intensity in different concentrations (see the Supporting Information). We found that when measuring in the same conditions, the values for all the helical complexes are close to that of $Ru(bipy)_3(PF_6)_2$ ($\Phi = 0.018$),[20] while the values are 3 or 9 times lower in the cases of Ru(**5SM**)$_3$ and Ru(**5PM**)$_3$, respectively (Table 1). As a control and another example of an unstructured flexible ligand, we synthesized the dimethylated version of the amine *N*bpm, [(4"-methyl-2',2"-bipyridine-4'-yl)-methyloxy]ethyl (dimethyl)amine (**bp-4DM**)[21] and its corresponding ruthenium

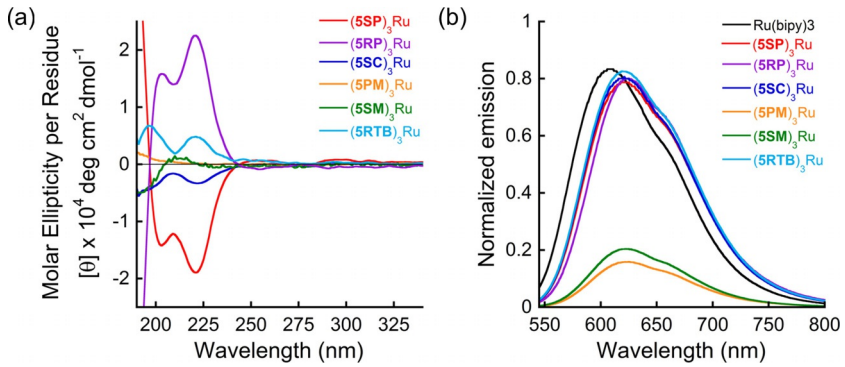

Figure 2. Structure–function relationships within Ru(peptoid pentamer)$_3$ complexes. a) CD spectra measured at rt. in acetonitrile: per residue molar ellipticity of Ru(**5SP**)$_3$, Ru(**5RP**)$_3$, Ru(**5SC**)$_3$, Ru(**5RTB**)$_3$, Ru(**5SM**)$_3$ and Ru(**5PM**)$_3$ (30 μM each). b) Normalized emission spectra of Ru(bipy)$_3$, Ru(**5SP**)$_3$, Ru(**5RP**)$_3$, Ru(**5SC**)$_3$, Ru(**5RTB**)$_3$, Ru(**5SM**)$_3$ and Ru(**5PM**)$_3$ (5 μM each in acetonitrile, in air, at RT).

complex Ru(**bp-4DM**)$_3$ (see the Supporting Information). The complex Ru(**bp-4DM**)$_3$ showed a luminescence intensity ten times lower than that of Ru(bipy)$_3$ as measured in acetonitrile in air at RT (see the Supporting Information), with $\Phi = 0.002$, an order of magnitude lower than that of Ru(bipy)$_3$ ($\Phi = 0.018$). Overall, these observations are remarkable because they suggest that only in some cases there is a specific interaction between the substituent on the ligand and the ruthenium center that leads to its quenching, and that these interactions are only possible when the ligand substituent is flexible and unstructured. Specifically, we identify a direct correlation between structure and function: the peptoids helicity and the luminescence of embedded ruthenium complexes.

Structure–function studies

At this point we aimed to understand the correlation between the structure of the Ru–peptoid complexes and their luminescence properties, as well as the factors that enable quenching only by unstructured flexible peptoids. A key question in this context is whether a single unstructured peptoid can cause emission quenching or is it a different structural arrangement created by the assembly of three peptoid oligomers by one ruthenium ion that enables the quenching. In other words, we wanted to know if the luminescence is actually dependent on the helicity (secondary structure) of the peptoid scaffold or on another, higher ordered, structure. To understand the influence of a single peptoid ligand on the emission properties of the corresponding ruthenium complex, we prepared the two heteroleptic ruthenium complexes, Ru(bipy)$_2$(**5SP**) and Ru(bipy)$_2$(**5PM**). The complexes were synthesized by treating one equivalent of peptoid with one equivalent of Ru(bipy)$_2$Cl$_2$ in refluxing ethanol under nitrogen atmosphere (see the Supporting Information). The complexes were precipitated with NH_4PF_6 and purified by HPLC. Interestingly, both Ru(bipy)$_2$(**5SP**) and Ru(bipy)$_2$(**5PM**) have comparable emission intensities (see the Supporting Information), very similar to that of Ru(bipy)$_3$. The quantum efficiencies of luminescence of Ru(bipy)$_2$(**5SP**) and Ru(bipy)$_2$(**5PM**) are $\Phi = 0.018$ and $\Phi = 0.016$, respectively. This is in contrast to the analogous homoleptic complexes Ru(**5SP**)$_3$ and Ru(**5PM**)$_3$ that show very different emission properties. From this experiment it is evident that one peptoid ligand is not sufficient to cause the luminescence quenching, thus the emission properties of the heteroleptic complex are not influenced by the secondary structure of the substituting peptoid ligand. These properties should therefore be a consequence of some higher-order arrangement of the three peptoid oligomers attached to each Ru(bipy)$_3$ center.

In the absence of crystals suitable for X-ray analysis, we decided to employ two different transmission electron microscopy (TEM) techniques, a conventional TEM and a high-resolution (HR) TEM; the latter is known to enable direct observation of three-dimensional peptoid structures.[22] We initially performed conventional TEM measurements with samples containing 10 μM Ru(**5SP**)$_3$, Ru(**5PM**)$_3$, Ru(**5SM**)$_3$ or Ru(**5RTB**)$_3$ in acetonitrile (the complexes are completely soluble) that were deposited on polymer-coated copper grids negatively stained with phosphotungstic acid. The grids were dried in air prior to analysis, leaving the Ru-bundle complexes adsorbed on the polymer. Figure 3a shows representative TEM images of Ru(**5RTB**)$_3$ and Ru(**5SP**)$_3$ (inset), in which worm-like assemblies with an average length of 77.8(±29.7) nm and 228.3(±78.5) nm, respectively, and an average width of 10.5(±3.6) nm and 25.2 (±6.33) nm, respectively, are inspected. Figure 3b presents the TEM image of Ru(**5SM**)$_3$, which shows sphere-like assemblies

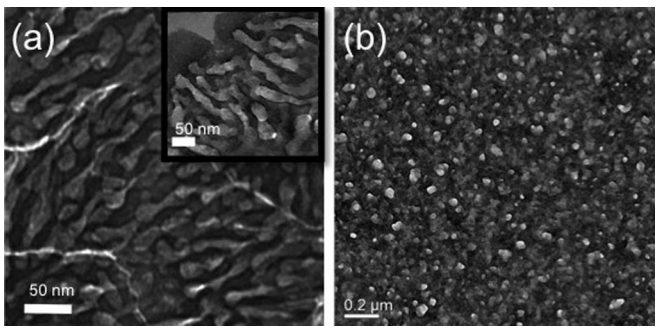

Figure 3. TEM images of samples containing 10 μM peptoids in acetonitrile that were deposited on polymer-coated copper grids negatively stained with phosphotungstic acid (yielding white-atom contrast). a) Ru(**5RTB**)$_3$ and Ru(**5SP**)$_3$ (inset), showing the formation of worm-like assemblies, and b) Ru(**5SM**)$_3$ oligomers assembled to spheres.

with an average diameter of 43.5(±10.32) nm. Interestingly, TEM analysis of Ru(**5PM**)$_3$ revealed mixed morphology containing both worm-like assemblies and spheres (Figure S74). These micrographs provide evidence that ruthenium complexes from both helical and unstructured peptoids form 3D arrangements with structure-dependent morphology.

To gain more information about the structural composition of the worm-like assemblies we performed HR-TEM measurements with the same solutions of Ru(**5RTB**)$_3$ or Ru(**5SP**)$_3$ that were used in the conventional TEM measurements. Samples from these solutions were deposited on holey carbon coated copper grids. The grids were dried in air prior to analysis. The obtained high-resolution images revealed great detail about the structural organization of the worm-like assemblies, showing individual chains that can represent either separate peptoid helices or bundles of three helices held via coordination to the embedded Ru(bipy)$_3$ complex (Figure 4 a, b).[23]

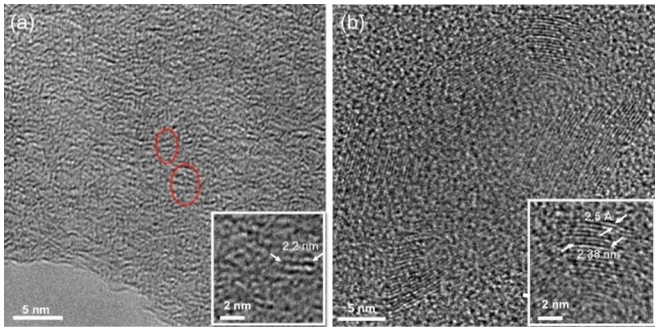

Figure 4. HR-TEM images of samples containing 10 μM peptoids in acetonitrile that were deposited on holey carbon copper grids, providing direct imaging (black-atom contrast) of: a) Ru(**5RTB**)$_3$ (Talos 200 C operated at 200 kV), and b) Ru(**5SP**)$_3$ (Titan Themis G^2 300 operated at 80 kV). Insets: magnified images of the individual metallopeptoids and metallopeptoid bundles (also marked in red in a).

The average chain length of 2.2–2.4 nm is in agreement with the length of an *N*r1tbe containing peptoid homopentamer, the crystal structure of which was recently published.[4l] Specific arrangements of helical bundles can be also observed (marked in red circles in Figure 4 a) with an average space width between peptoids of 2.5 Å (marked by two white pointing arrows in the inset of Figure 4 b), which can be assigned to hydrophobic interactions and/or π–π stacking between helices from the same bundle. Energy-dispersive X-ray spectroscopy (EDS) analysis performed on a sample containing Ru(**5RTB**)$_3$ confirmed the presence of ruthenium in this sample (Figure S75). The ATR-FT IR spectra of Ru(**5RTB**)$_3$ and Ru(**5SP**)$_3$ measured from the TEM solutions before and after these were dried, were similar for each peptoid (Figure S76), suggesting that the structures seen in the TEM images are also present in solution.

These results, together with the luminescence data provide a strong and remarkable confirmation for the direct relationship between structure and function within these Ru–peptoid complexes. Previous studies on peptides bearing amino acid chromophores demonstrated that the peptide bond itself is an intramolecular quencher and that the fluorescence decay depends on local backbone conformations about the chromophore moiety.[20] It was also suggested that the backbone carbonyl group can act as a fluorescent quencher of indole chromophores.[21] This quenching occurs via a through-space electron transfer mechanism, which depends on the number, distance, and possibly the orientation of peptide bonds about the indole ring.[10,22] It is also known that amines can quench the emission of Ru(bipy)$_3$ complexes depending on their concentration, structure and on the solvent.[23] The peptoid backbone contains amide, carbonyl and amine groups, thus, the quenching of the luminescence that is observed when unstructured peptoid ligands coordinate to the ruthenium ion may be attributed to the through-space interactions of the peptoid backbone with the ruthenium center. Our hypothesis is, that in the case of helical peptoid ligands, a more rigid structure is formed keeping the peptoid backbone far apart from the metal center, thus minimizing the interaction of the peptoid scaffold with the ruthenium center (Figure 5 a). In contrast,

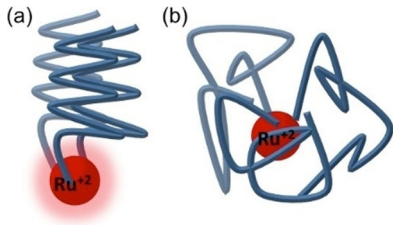

Figure 5. A cartoon representing our hypothesis regarding the formation of either Ru^{2+} complexes from: a) three helical peptoids, which do not interact with the ruthenium center, or from b) three unstructured flexible ligands that can interact with the ruthenium center leading to through-space quenching.

when unstructured peptoids are coordinated, the metal center is surrounded and possibly covered by the peptoid ligands, which can interact with the peptoid backbone, resulting in through-space luminescence quenching (Figure 5 b). This hypothesis is supported by the TEM images presented in Figure 3 and Figure 4, showing elongated structures in the case of helical pepetoids and spherical structures in the case of unstructured peptoids, as well as by the results obtained in case of the complex Ru(**bp-4DM**)$_3$ (see above) in which the luminescence of the ruthenium center is also quenched by its interactions with the flexible ligand that contains amine groups.

Sequence–structure–function relationships

It is known from previous research that the degree of peptoid helicity depends on their length and monomer sequence. In order to further explore our intriguing observations we wanted to see if we can actually tune the function (luminescence) of phenylethyl Ru–peptoid complexes by systematically altering the helicity of Ru(**5SP**)$_3$. To do so, we first examined the CD spectra and luminescence properties of ruthenium complexes based on *N*spe peptoids different in their chain length, namely Ru(**2SP**)$_3$, Ru(**3SP**)$_3$, and Ru(**7SP**)$_3$. The CD spectra of the free peptoids (see the Supporting Information) and

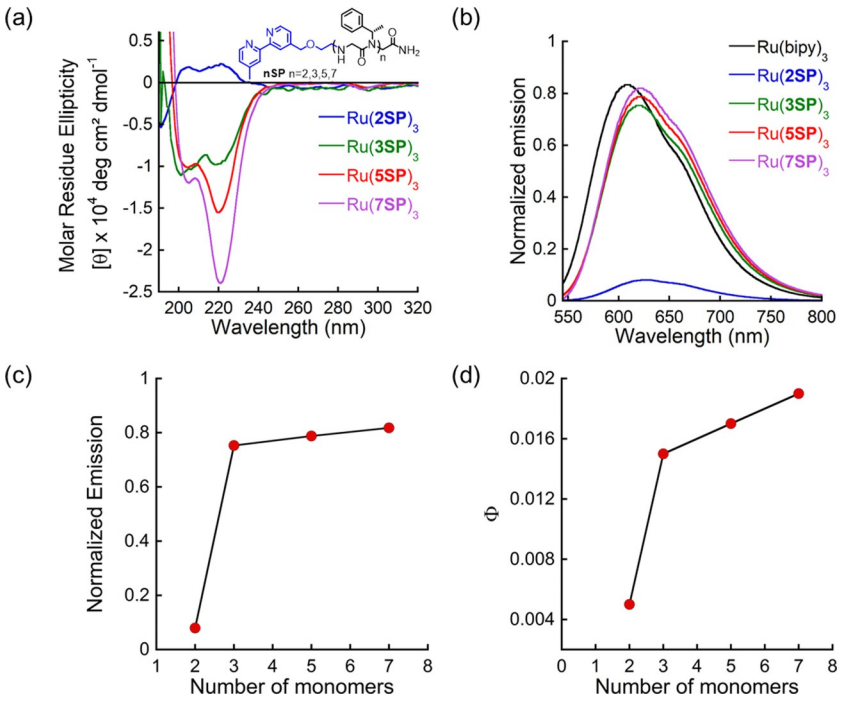

Figure 6. Peptoid chain length dependent luminescence in *N*spe–peptoid–Ru complexes. a) CD spectra of Ru(**2SP**)$_3$, Ru(**3SP**)$_3$, Ru(**5SP**)$_3$, Ru(**7SP**)$_3$ (30 μM each in acetonitrile). b) Normalized luminescence spectra of Ru(bipy)$_3$, Ru(**2SP**)$_3$, Ru(**3SP**)$_3$, Ru(**5SP**)$_3$ and Ru(**7SP**)$_3$ (5 μM in acetonitrile). c) Normalized emission versus the number of monomers Ru(**nSP**)$_3$. d) Luminescence quantum efficiency versus number of monomers Ru(**nSP**)$_3$.

their ruthenium complexes (Figure 6a) were recorded in acetonitrile at room temperature. As expected, the CD spectrum of Ru(**2SP**)$_3$ displayed only weak CD signals, indicating no helical secondary structure. This is in line with the previous observation that at least three monomers are required in order to form helical secondary structure with a helical pitch of three residues per turn.[4b] The CD signal of Ru(**3SP**)$_3$ has a lower intensity than the signal measured for Ru(**5SP**)$_3$, with double minima of equal intensity at 200 nm and 220 nm, suggesting that this has a helical structure with an equal population of *cis* and *trans* amide bonds.[4c] The CD spectra of Ru(**7SP**)$_3$ shows the strongest signal with an intensity by 66% higher than that of Ru(**5SP**)$_3$. The major band was observed at 220 nm, indicating a higher population of *cis* amide bonds.

The emission spectrum at the range of 550–800 nm was measured for these three complexes upon irradiation at 450 nm (Figure 6b) and the quantum efficiency of luminescence was experimentally derived. The complex Ru(**7SP**)$_3$ demonstrates the highest emission intensity, comparable to that of Ru(bipy)$_3$. The emission intensity is slightly diminished when decreasing the length of the helical peptoid scaffold from seven monomers in Ru(**7SP**)$_3$ to five monomers in Ru(**5SP**)$_3$ and to three monomers in Ru(**3SP**)$_3$ (Figure 6b). For the unstructured dimer **2SP**, the emission intensity of the corresponding ruthenium complex Ru(**2SP**)$_3$ is lower by an order of magnitude compared to that of Ru(**7SP**)$_3$, Ru(**5SP**)$_3$ and Ru(**3SP**)$_3$ (Figure 6b). The same trend is observed for the value of Φ, which is 0.005 for Ru(**2SP**)$_3$—three to four times lower than the values measured for Ru(**7SP**)$_3$ (0.019), Ru(**5SP**)$_3$ (0.017) and Ru(**3SP**)$_3$ (0.015). From the chain-length dependence plots (Figure 6c, d) we can conclude that the luminescence is a chain length dependent property with the critical chain length of three monomers. Below this length, the luminescence is quenched and above this length, the peptoid scaffold adopts a helical secondary structure and the luminescence is maintained and only slightly enhanced with the increase in the peptoid chain length.

Following these observations, we decided to modify the sequence of **5SP** by using a combination of chiral *N*spe groups and nonchiral *N*pm groups incorporated at different positions along the peptoid sequence (Figure 1b). Based on previous experience, we expect that the position and number of the *N*spe groups should affect the helicity of the peptoid[16,28] and its metal complex,[28] thus we aimed to probe the influence of the change in helicity of the peptoid scaffold on the luminescence of the corresponding ruthenium complex. We synthesized four peptoid oligomers all bearing an *N*bpm group at the terminal 5th position but have different combination of *N*spe and *N*pm groups. Oligomer **5SP1** has one *N*spe group at the 1st position, oligomer **5SP1_2** has two *N*spe groups at the 1st and 2nd positions and oligomers **5SP4** and **5SP3_4** have one *N*spe groups at the 4th and two *N*spe groups at the 3rd and 4th positions, respectively. The corresponding ruthenium complexes Ru(**5SP1**)$_3$, Ru(**5SP1_2**)$_3$, Ru(**5SP4**)$_3$ and Ru(**5SP3_4**)$_3$ were synthesized according to the usual procedure and their CD spectra and luminescence properties were measured (Figure 7a and b, respectively).

The CD spectrum of complex Ru(**5SP1**)$_3$ shows a signal with an intensity three times lower than that of Ru(**5SP**)$_3$ with double minima of nearly equal intensity at about 200 nm and

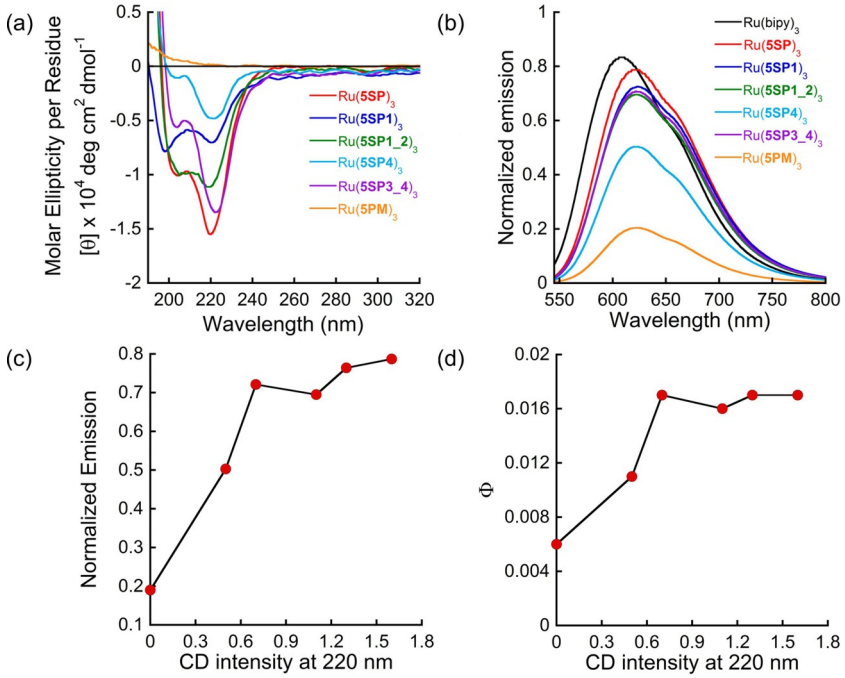

Figure 7. Sequence and structure-dependent luminescence in phenyl Ru–peptoid complexes. a) CD spectra of Ru(**5SP**)$_3$, Ru(**5SP1**)$_3$, Ru(**5SP1_2**)$_3$, Ru(**5SP4**)$_3$, Ru(**5SP3_4**)$_3$ and (**5PM**)$_3$Ru (30 μM each in acetonitrile). b) Normalized luminescence spectra of Ru(bipy)$_3$, Ru(**5SP**)$_3$, Ru(**5SP1**)$_3$, Ru(**5SP1_2**)$_3$, Ru(**5SP4**)$_3$, Ru(**5SP3_4**)$_3$ and Ru(**5PM**)$_3$ (5 μM in acetonitrile). c) Normalized emission versus CD intensity at 220 nm of all six Ru–peptoid complexes. d) Luminescence quantum efficiency versus CD intensity at 220 nm of all six Ru–peptoid complexes.

220 nm, consistent with the initiation of a helical structure. The CD spectrum of Ru(**5SP1_2**)$_3$ has a similar shape but with twice as high an intensity, consistent with a more pronounced helical structure. The CD spectrum of Ru(**5SP4**)$_3$ shows a very low intensity pick near 220 nm while that of Ru(**5SP3_4**)$_3$ exhibits a signal with similar intensity to Ru(**5SP**)$_3$ but with the larger peak at around 220 nm, suggesting an overall helical structure of the peptoid with a higher population of *cis* amide bonds. The complex Ru(**5SP4**)$_3$ shows the lowest luminescence intensity with a value located between that of the completely disordered Ru(**5PM**)$_3$ and the helical Ru(**5SP**)$_3$ (Figure 4b). Complexes Ru(**5SP1**)$_3$, Ru(**5SP1_2**)$_3$ and Ru(**5SP3_4**)$_3$, show luminescence intensity slightly lower than that of Ru(**5SP**)$_3$, and very close in value to one another.

Overall, we could demonstrate a clear trend pointing at increased luminescence intensity (or quenching) as a function of the peptoid scaffold helicity; as the peptoid is less structured, it can enable more efficient quenching of the Ru(bipy)$_3$ center and as it is more helical, showing increased intensity of the CD band near 220 nm, the luminescence of the Ru(bipy)$_3$ center increases as well (Figure 7c). The experimental values of quantum efficiency for complexes Ru(**5SP1**)$_3$, Ru(**5SP1_2**)$_3$, Ru(**5SP4**)$_3$ and Ru(**5SP3_4**)$_3$ support this trend with the values of $\Phi = 0.017$, $\Phi = 0.016$, $\Phi = 0.011$ and $\Phi = 0.016$, respectively (Table 1 and Figure 7d). Moreover, tuning of luminescence could also be achieved, as we observed significant differences in luminescence corresponding with the different degrees of helicity of the various peptoid ligands. The emission lifetimes (see Table 1) of all peptoid complexes are close to that of Ru(bipy)$_3$(PF$_6$)$_2$ (0.156 μs) as measured in acetonitrile in air at room temperature and are at the typical range of Ru(bipy)$_3$ complexes in air.[17]

Remote induced chirality from the chiral peptoid monomers to the achiral Ru(bipy)$_3$ center

It was previously shown that the chirality of Ru(bipy)$_3$ complexes could be resolved by attaching a helical scaffold to the bipy ligand, which allows the predetermination of the complex chirality.[19,29] As discussed above, all the Ru–peptoid complexes produce absorption bands near 285 and 460 nm; an example of UV/Vis spectra of **5SP** and its Ru complex is depicted in Figure 8a. Ruthenium binding to **5SP** also produces a new band in the CD spectrum, of very low intensity at about 295 nm corresponding to the π–π* transition of the bipy ligand. This band is very weak and does not show the expected Cotton effect. Repeating the measurement at higher concentrations (300 μM vs. 30 μM) resulted in a stronger CD signal that showed clear Cotton effect with a minimum at 293 nm (Figure 8b, red line). CD measurements at even higher concentrations (1.5 mM) in the wavelength range of 400–600 nm show a 75 nm wide exciton couplet with a crossing point at 450 nm, which is related to the wavelength of the MLCT band (Figure 8c, red line).

The directionality of the band corresponds to Δ absolute configuration at the metal center.[30] These signals reflect the induction of chirality from the peptoid scaffold to the metal center resulting in the stereoselective formation of the Δ stereoisomer. As expected, the CD spectra of the corresponding complex Ru(**5RP**)$_3$ in the high concentrations show inversed

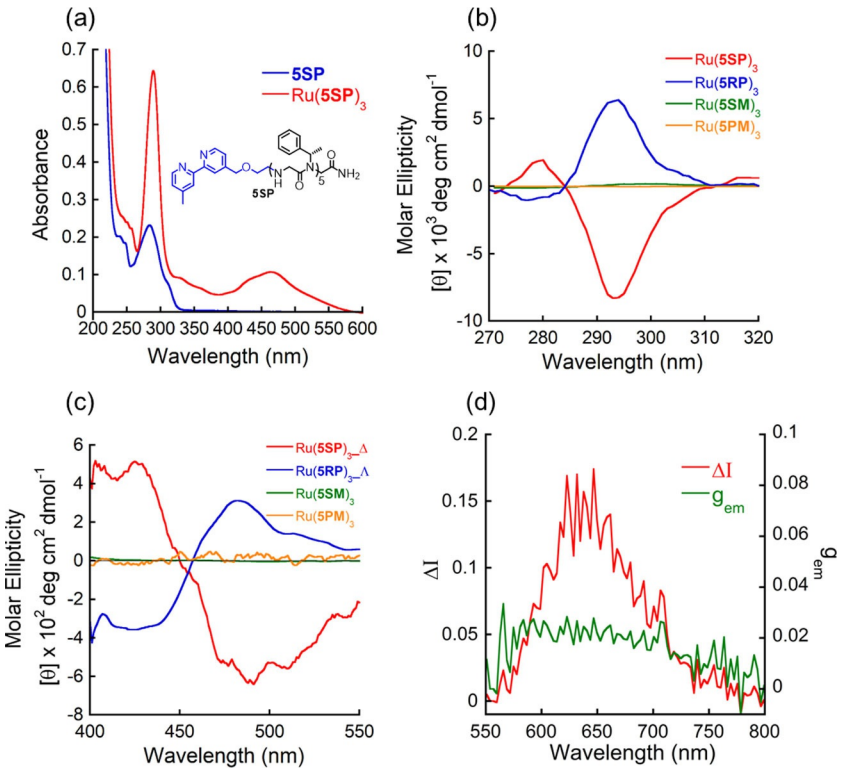

Figure 8. Chiral induction from helical peptoid pentamers. a) UV/Vis spectra of **5SP** (30 μM in acetonitrile) and Ru(**5SP**)$_3$ (10 μM in acetonitrile). b) CD spectra measured at RT. of Ru(**5SP**)$_3$, Ru(**5RP**)$_3$, Ru(**5SM**)$_3$ and Ru(**5PM**)$_3$ (300 μM in acetonitrile). c) CD spectra at RT of the four complexes above (1.5 mM in acetonitrile). d) CPL spectrum and emission dissymmetry values of Ru(**5SP**)$_3$ (500 μM in acetonitrile in air).

signals to those of Ru(**5SP**)$_3$ at the near UV and the far UV regions (Figure 8b, c, blue lines). The exciton couplet of Ru(**5RP**)$_3$ at 450 nm corresponds to that of a Λ ruthenium complex.[31] These results support the observation that the stereochemistry of the formed ruthenium complex is dictated by the chirality of the peptoid scaffold and the handedness of the peptoid helix. Both Ru(**5SC**)$_3$ and Ru(**5RTB**)$_3$ also produced bands in the CD spectra at the near UV and the far UV regions (see the Supporting Information). The CD spectrum of Ru(**5SC**)$_3$ exhibits two intense exciton couplets at the wavelength range of 270–310 nm and 400–600 nm, similar to those of Ru(**5RP**)$_3$ suggesting the formation of a Λ ruthenium complex. The spectrum of Ru(**5RTB**)$_3$ is very similar to this of Ru(**5RP**)$_3$, with a band near 293 nm and an exciton couplet near 450 nm, also suggesting the formation of a Λ ruthenium complex. Interestingly, the CD spectra of Ru(**5SM**)$_3$, which is composed of a chiral peptoid, do not show any signals at 290 nm and 450 nm even at higher concentrations indicating no induction of chirality from the chiral *N*smp substituents to the metal center (Figure 8b, c, green line). As expected, no CD spectra was obtained for Ru(**5PM**)$_3$, which is a completely achiral complex.

The photoluminescence of Ru(**5SP**)$_3$ allows us to measure its circularly polarized luminescence (CPL) spectrum. CPL is a spectroscopic technique for measuring the differential emission of left and right circularly polarized light. The obtained spectrum reflects the chirality of the complex in its luminescent (excited) state. CPL is quantitatively expressed by the emission anisotropy factor, g_{em}, also known as the dissymmetry factor, which can be calculated according to Equation (1). The CPL spectrum of Ru(**5SP**)$_3$ is depicted in Figure 8d. Ru(**5SP**)$_3$ has a g_{em} value of 1.9×10^{-2} [±0.1]. Typical values of the dissymmetry factor for chiral, luminescent organic molecules and chiral, luminescent transition metal complexes are in the 10^{-2}–10^{-5} order of magnitude.[32]

$$g_{em}(\lambda) = \frac{\Delta I}{0.5I} = \frac{I_L - I_R}{0.5(I_L + I_R)} \quad (1)$$

The complex shows a slight decrease in g_{em} as the wavelength increases, consistent with previous work conducted on Ru(bpy)$_3^{2+}$ complexes.[32] The CPL measurement of Ru(**5SM**)$_3$ was also recorded and it supports the observation that there is no chirality induction from the chiral *N*smp substituents to the ruthenium center as its dissymmetry factor is $g_{em}=0$ (see the Supporting Information). Thus, the monomers chirality by itself is not sufficient to induce chirality on the metal center and the helicity of the entire structure is required.

Chiral induction could also be observed from the CD spectra of Ru(**3SP**)$_3$ and Ru(**7SP**)$_3$ measured at high concentrations, with bands at near 290 nm (in 300 μM solution) and an exciton couplet at 400–600 nm region (in 1.5 mM). While no bands were detected in the CD spectrum of Ru(**2SP**)$_3$ even at high concentrations (Figure 9a). Moreover, the intensity of the signal at 280 nm correlates with the intensity of the signal at 200–220 nm. Thus, the intensity of the signal is elevated with the increase in peptoid length. The absence of a Cotton effect

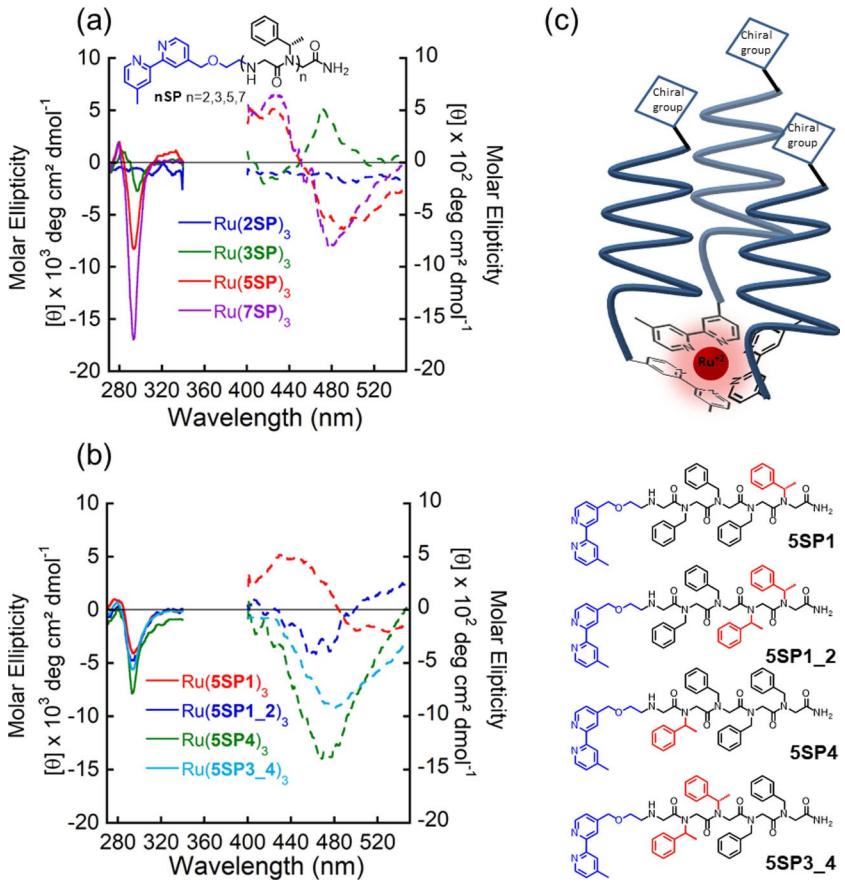

Figure 9. a) CD spectra measured at RT in acetonitrile of Ru(**2SP**)$_3$, Ru(**3SP**)$_3$, Ru(**5SP**)$_3$ and Ru(**7SP**)$_3$ (300 μM, full lines and 1.5 mM, dashed lines). b) CD spectra measured at RT in acetonitrile of Ru(**5SP1**)$_3$, Ru(**5SP1_2**)$_3$, Ru(**5SP4**)$_3$ and Ru(**5SP3_4**)$_3$ (300 μM, full lines and 1.5 mM, dashed lines). c) Schematic representation of the chiral induction on the ruthenium metal center. Even one remote chiral group is sufficient to obtain chirality at the metal center.

signal for Ru(**2SP**)$_3$ at about 280 nm, indicates that the chiral induction is caused by the helical structure of the peptoid scaffold rather than by the chirality of the single *N*spe monomer that is present in Ru(**2SP**)$_3$. Additional CD measurements revealed that the spectrum of the heteroleptic complex Ru(bipy)$_2$(**5SP**) is similar to this of Ru(**5SP**)$_3$, while the spectrum of Ru(bipy)$_2$(**5PM**) did not show any signals (see the Supporting Information). The complexes Ru(**5SP1**)$_3$, Ru(**5SP1_2**)$_3$, Ru(**5SP4**)$_3$ and Ru(**5SP3_4**)$_3$ all exhibit pronounced Cotton effect near 290 nm and exciton couplets at the 400–600 nm region, implying a preferable Δ stereochemistry (Figure 9b). Notably, in the cases of complexes Ru(**5SP1**)$_3$ and Ru(**5SP1_2**)$_3$, there is a remote chiral induction on the metal center through a chain of three (four amide bonds) or two (three amide bonds) achiral *N*pm monomers (through 21 or 18 bonds, respectively), a phenomena that was previously observed only for peptide substituted bipyridyl iron complexes.[33]

Conclusions

Despite the well-established relationships between sequence, structure and function in biopolymers, knowledge about these relationships in peptoids and other peptide mimics is still lacking, hampering their usage in various applications. Thus, the demonstration of a direct correlation between structure and function by helical peptoid oligomers is a milestone in the development of biomimetic foldamers. In this work, we explore these relationships and show, for the first time, that the luminescence intensity of ruthenium centers embedded within peptidomimetic scaffolds, can be controlled solely by the structure of the oligomer, specifically its helicity. Based on circular dichroism and fluorescence spectroscopy we demonstrate that while helical peptoids do not affect the fluorescence of the embedded Ru^{II} center, unstructured peptoids lead to its significant decay. TEM measurements revealed that ruthenium binding to either helical or unstructured peptoids results in elongated or spherical assemblies, respectively, suggesting that only the latter can interact with the ruthenium dye resulting in through-space luminescence quenching. Further HR-TEM analysis enabled the remarkable direct imaging of individual ruthenium-bound peptoids and bundles. We also demonstrated that by simple modifications to one peptoid sequence, which lead to variations in its helical structure, we could fine-tune the luminescence properties of the embedded ruthenium complexes. Finally, we could achieve remote chiral induction over up to four amide bonds from the peptoid backbone to the ruthenium center, as was indicated from CD and CPL spectroscopies. We believe that this unique correlation between secondary/tertiary structure of synthetic oligomers and the two fundamental properties luminescence and chirality, is

not only an additional tool for studying structure–function relationships in peptidomimetics but also holds great potential for applications in chemical biology, photocatalysis, molecular imaging and more.

Acknowledgements

This research was funded by the Solar Fuels Israel Center of Research Excellence (I-CORE) of the Israeli Science Foundation (ISF), grant number 2018762. We thank Mrs. Larisa Panz for her assistance with the various MS measurements, Mrs. Rotem Strassberg from the group of Prof. Efrat Lifshitz at the Schulich faculty of Chemistry, Technion, for the CPL measurements, Dr. Lior Gal and Tzach Jaffe from the group of Prof. Meir Orenstein at the Electrical Engineering Faculty, Technion, for the Fluorescence decay measurements, and to Mrs. Anastasia Golovetski for the IR measurements.

Conflict of interest

The authors declare no conflict of interest.

Keywords: foldamers · helix · induced chirality · peptides · peptidomimetics

[1] a) G. Maayan, *Eur. J. Org. Chem.* **2009**, 5699 – 5710; b) G. Maayan, M. Albrecht in *Metallofoldamers: Supramolecular Architectures from Helicates to Biomimetics*, Wiley, **2013**.
[2] a) Z. C. Girvin, S. H. Gellman, *J. Am. Chem. Soc.* **2018**, *140*, 12476 – 12483; b) R. Brimioulle, D. Lenhart, M. Maturi, M. T. Bach, *Angew. Chem. Int. Ed.* **2015**, *54*, 3872 – 3890; *Angew. Chem.* **2015**, *127*, 3944 – 3963.
[3] J. Crassous, *Chem. Soc. Rev.* **2009**, *38*, 830 – 845.
[4] a) K. Kirshenbaum, A. Barron, E. Goldsmith, R. A. Armand, P. Bradley, E. K. T. V. Truong, K. A. Dill, F. E. Cohen, R. N. Zuckermann, *Proc. Natl. Acad. Sci. USA* **1998**, *95*, 4303 – 4308; b) C. W. Wu, T. J. Sanborn, R. N. Zuckermann, A. E. Barron, *J. Am. Chem. Soc.* **2001**, *123*, 2958 – 2963; c) C. W. Wu, T. J. Sanborn, K. Huang, R. N. Zuckermann, A. E. Barron, *J. Am. Chem. Soc.* **2001**, *123*, 6778 – 6784; d) C. W. Wu, K. Kirshenbaum, T. J. Sanborn, J. A. Patch, K. Huang, K. A. Dill, R. N. Zuckermann, A. E. Barron, *J. Am. Chem. Soc.* **2003**, *125*, 13525 – 13530; e) B. C. Gorske, B. L. Bastian, G. D. Geske, H. E. Blackwell, *J. Am. Chem. Soc.* **2007**, *129*, 8928 – 8929; f) N. H. Shah, G. Butterfoss, L. Nguyen, K. Yoo, B. R. Bonneau, D. L. Rabenstein, K. Kirshenbaum, *J. Am. Chem. Soc.* **2008**, *130*, 16622 – 16632; g) B. C. Gorske, J. R. Stringer, B. L. Bastian, S. A. Fowler, H. E. Blackwell, *J. Am. Chem. Soc.* **2009**, *131*, 16555 – 16567; h) O. Roy, C. Caumes, Y. Esvan, C. Didierjean, S. Faure, C. Taillefumier, *Org. Lett.* **2013**, *15*, 2246 – 2249; i) C. Caumes, O. Roy, S. Faure, C. Taillefumier, *J. Am. Chem. Soc.* **2012**, *134*, 9553 – 9956; j) J. R. Stringer, J. A. Crapster, I. A. Guzei, H. E. Blackwell, *J. Am. Chem. Soc.* **2011**, *133*, 15559 – 15567; k) J. A. Crapster, I. A. Guzei, H. E. Blackwell, *Angew. Chem. Int. Ed.* **2013**, *52*, 5079 – 5084; *Angew. Chem.* **2013**, *125*, 5183 – 5188; l) O. Roy, G. Dumonteil, S. Faure, L. Jouffret, A. Kriznik, C. Taillefumier, *J. Am. Chem. Soc.* **2017**, *139*, 13533 – 13540.
[5] a) K. J. Prathap, G. Maayan, *Chem. Commun.* **2015**, *51*, 11096 – 11099; b) M. Baskin, G. Maayan, *Chem. Sci.* **2016**, *7*, 2809 – 2820.
[6] G. Maayan, M. D. Ward, K. Kirshenbaum, *Proc. Natl. Acad. Sci. USA* **2009**, *106*, 13679 – 13684.
[7] Y. Shen, C. F. Chen, *Chem. Rev.* **2012**, *112*, 1463 – 1535.
[8] T. Biet, K. Martin, J. Hankache, N. Hellou, A. Hauser, T. Bergi, A. T. Vanthuyne, M. Caricato, J. Crassous, N. Avarvari, *Chem. Eur. J.* **2017**, *23*, 437 – 446.
[9] R. B. Prince, J. G. Saven, P. G. Wolynes, J. S. Moore, *J. Am. Chem. Soc.* **1999**, *121*, 3114 – 3121.
[10] a) J. R. Lakowicz, *Principles of Fluorescence Spectroscopy*, **1999**, Academic/Plenum Publishers, New York; b) M. R. Eftink, *Intrinsic Fluorescence of Proteins, in Topics in Fluorescence Spectroscopy* (Ed.: J. R. Lakowicz), Kluwer Academic/Plenum Publishers, New York, **2000**, pp. 1 – 15.
[11] a) A. A. Fuller, F. J. Seidl, P. A. Bruno, M. A. Plescia, K. S. Palla, *Pept. Sci.* **2011**, *96*, 627 – 638; b) A. A. Fuller, C. A. Holmes, F. J. Seidl, *Pept. Sci.* **2013**, *100*, 380 – 386.
[12] a) C. Penas, E. Pazos, J. L. Mascareñas, M. E. Vázquez, *J. Am. Chem. Soc.* **2013**, *135*, 3812 – 3814; b) H. Wu, Y. Zhou, L. Yin, C. Hang, X. Li, H. Ågren, T. Yi, Q. Zhang, L. Zhu, *J. Am. Chem. Soc.* **2017**, *139*, 785 – 791.
[13] S. Campagna, F. Puntoriero, F. Nastasi, G. Bergamini, V. Balzani, *Photochemistry and Photophysics of Coordination Compounds: Ruthenium; in: Photochemistry and Photophysics of Coordination Compounds I, Topics in Current Chemistry* (Eds.: V. Balzani, S. Campagna), **2007**, *Vol. 280*, Springer, Heidelberg.
[14] G. Maayan, B. Yoo, K. Kirshenbaum, *Tetrahedron Lett.* **2008**, *49*, 335 – 338.
[15] M. Baskin, G. Maayan, *Biopolymers* **2015**, *104*, 577 – 584.
[16] H. M. Shin, C. M. Kang, M. H. Yoon, J. Seo, *Chem. Commun.* **2014**, *50*, 4465 – 4468.
[17] A. Juris, V. Balzani, *Coord. Chem. Rev.* **1988**, *84*, 85 – 277.
[18] R. N. Zuckermann, J. M. Kerr, S. B. W. Kent, W. H. Moos, *J. Am. Chem. Soc.* **1992**, *114*, 10646 – 10647.
[19] M. Baskin, L. Panz, G. Maayan, *Chem. Commun.* **2016**, *52*, 10350 – 10353.
[20] K. Suzuki, A. Kobayashi, S. Kaneko, K. Takehira, T. Yoshihara, H. Ishida, Y. Shiina, S. Oishi, S. Tobita, *Phys. Chem. Chem. Phys.* **2009**, *11*, 9850 – 9860.
[21] L. J. Strekowski, F. L. Tanious, R. A. Watson, D. Harden, M. W. Mokrosz, D. Edwards, W. D. Wilson, *J. Med. Chem.* **1988**, *31*, 1231 – 1240.
[22] S. A. Shelby, A. B. Marciel, P. C. Choi, R. Chen, L. Tan, T. K. Chu, R. A. Mesch, B. C. Lee, M. D. Connolly, C. Kisielowski, R. N. Zuckermann, *Nat. Mater.* **2010**, *9*, 454 – 460.
[23] a) M. R. Ghadiri, C. Soares, C. Choi, *J. Am. Chem. Soc.* **1992**, *114*, 825 – 831; b) M. R. Ghadiri, M. A. Case, *Angew. Chem. Int. Ed. Engl.* **1993**, *32*, 1594 – 1597; *Angew. Chem.* **1993**, *105*, 1663 – 1670; c) M. A. Case, M. R. Ghadiri, M. W. Mutz, G. L. McLendon, *Chirality* **1998**, *10*, 35 – 40.
[24] C. A. Royer, *Chem. Rev.* **2006**, *106*, 1769 – 1784.
[25] Y. Chen, B. Liu, H. T. Yu, M. D. Barkley, *J. Am. Chem. Soc.* **1996**, *118*, 9271 – 9278.
[26] R. W. Alston, M. Lasagna, G. R. J. Grimsley, M. Scholtz, G. D. Reinhart, C. N. Pace, *Biophys. J.* **2008**, *94-95*, 2280 – 2287.
[27] a) H. A. Garrera, J. J. Cosa, C. M. Previtali, *J. Photochem. Photobiol. A* **1989**, *47*, 143 – 153; b) C. R. Rivarola, S. G. Bertolotti, C. M. Previtali, *J. Photochem. Photobiol. A* **2006**, *82*, 213 – 218.
[28] L. Zborovsky, A. Smolyakova, M. Baskin, G. Maayan, *Chem. Eur. J.* **2018**, *24*, 1159 – 1167.
[29] J. Crassous, *Chem. Commun.* **2012**, *48*, 9684 – 9692.
[30] S. G. Telfer, T. M. McLean, M. R. Waterland, *Dalton Trans.* **2011**, *40*, 3097 – 3108.
[31] J. Kumar, T. Nakashima, T. Kawai, *J. Phys. Chem. Lett.* **2015**, *6*, 3445 – 3452.
[32] a) A. Gafni, I. Z. Steinberg, *Isr. J. Chem.* **1977**, *17*, 102 – 105; b) T. Biet, T. Cauchy, Q. Sun, J. Ding, A. Hauser, P. Oulevey, T. Bürgi, D. Jacquemin, N. Vanthuyne, J. Crassous, N. Avarvari, *Chem. Commun.* **2017**, *53*, 9210 – 9213.
[33] N. Ousaka, Y. Takeyama, H. Iida, E. Yashima, *Nat. Chem.* **2011**, *3*, 856 – 861.

Manuscript received: March 31, 2019
Revised manuscript received: May 1, 2019
Accepted manuscript online: May 2, 2019
Version of record online: June 11, 2019